# Journal of Materials Chemistry A

Accepted Manuscript


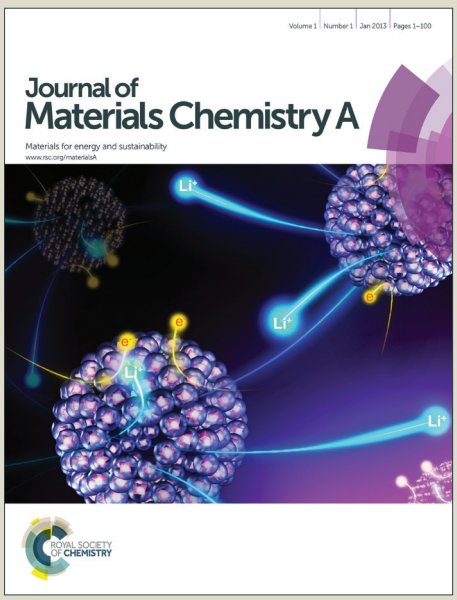





ROYAL SOCIETY OF CHEMISTRY

www.rsc.org/materialsA

Journal Name

RSCPublishing

ARTICLE

# Spontaneous interlayer formation in OPVs by additive migration due to additive-metal interactions

Cite this: DOI: 10.1039/xoxxoooooox

Igal Deckman,[a] Moshe Moshonov,[a] Stas Obuchovsky,[a] Reuven Brener,[b] and Gitti L. Frey [a]

Received ooth January 2012,
Accepted ooth January 2012

DOI: 10.1039/xoxxoooooox

www.rsc.org/

The presence of interlayers between the active layer and the electrode are known to modify the metal work-function and enhance carrier extraction, consequently improving OPV device performance. Spontaneous formation of interlayers by surface-enrichment of suitable additives eliminates separate processing steps and hence is technically advantageous and cost effective. However, surface enrichment is limited to additives with low surface energy. Here we show that additive migration to the organic/electrode interface could be induced by additive-metal interactions, modulated by the interactions between the additive and the underlying substrate. In this study, additive migration induced by metal evaporation is studied by blending P3HT with PEG, an established interlayer material with a surface energy higher than that of P3HT. XPS analysis reveals that, as expected, PEG is not present on the surface of the organic spun film. However, Ca or Al evaporation induces a significant migration of PEG to the organic/metal interface. In contrast, Au evaporation does not induce such migration. The comparison between Al, Ca and Au, metals with significantly different reduction potentials revealed that the driving force for PEG migration is its chemical interaction with the deposited metal atoms. The extent of PEG migration was also found to depend on the type of the underlying substrate, ITO/PEDOT:PSS or ITO. Finally, the PEG interlayer is shown to reduce the Al work function confirming that spontaneous additive migration induced by metal-additive interactions could be harnessed for charge extraction in organic electronic devices.

## Introduction

The quest for renewable energy sources has generated major efforts in the scientific and industrial communities, with solar energy offering a clean and abundant alternative to fossil fuels. In this context, organic photovoltaics (OPV) is a particularly promising technology by virtue of its low-cost, large-scale, lightweight, flexible and reel-to-reel manufacturability. The current state-of-the-art polymer solar cells have reached the level of feasibility for commercialization by exceeding 10% power-conversion efficiency.[1] This significant breakthrough in the efficiency was achieved primarily by introducing the bulk-heterojunction (BHJ) concept, i.e. through-film interpenetrating continuous networks and segregated domains of a polymeric electron donor and a fullerene-derivative electron acceptor.[2] This morphology, in combination with the use of charge-selective electrodes, enhances the efficiency of charge generation and charge collection, respectively.

The morphology of the active layer and the carrier selectivity at the electrodes can be controlled by the use of additives.[3] Generally, three types of additives have been suggested, each associated with a specific contribution to the OPV device performance. Processing additives dictate the film morphology by inducing phase separation and/or crystallinity, consequently enhancing charge generation and/or charge transport.[4-7] Optically active additives, the second type, enhance charge generation by increasing the light absorption.[8-10] The third type of additives enhances charge collection by forming a layer between the active film and the electrode (often termed buffer layer or interlayer). This interlayer is either selective to one type of carrier or modifies the electrode work function.[11-14] It has been shown that the interlayers enhance device performance by increasing the open circuit voltage, Voc, and/or the short circuit current, Jsc. [15, 16]

Interlayers in OPVs are commonly deposited between the active layer and the electrodes in distinct processing steps, either before (bottom contact) or after (top contact) the deposition of the active layer. Processing techniques include thermal deposition in high vacuum and spin coating using solvents that do not dissolve the BHJ.[17, 18] It is widely accepted that eliminating these additional processing steps would be

advantageous to the fabrication of OPV devices. Recently, a few studies have reported the utilization of additive migration (surface segregation) towards the film surface to spontaneously form an interlayer.[19-22] For example, a small amount of a fluorocarbon fullerene additive, F-PCBM, was added to a solution of the commonly used BHJ components: poly(3-hexylthiophene-2,5-diyl) (P3HT) and Phenyl-C61-butyric acid methyl ester (PCBM). The F-PCBM was found to enrich the surface of the BHJ film and improve the photovoltaic device performance.[23, 24]

In a recent report we have demonstrated a different mechanism leading to the generation of such interlayers, namely the interlayer is formed upon the evaporation of the metal electrode onto the blend film. The usefulness of this method was epitomised for P3HT:PCBM:PEG blends where PEG molecules spontaneously migrated from the bulk film to the organic/metal interface during Al deposition. The PEG interlayer reduced the barrier for electron extraction and dramatically enhanced the OPV device performance.[25] We are aware of the ambiguity of the terms *spontaneous* while the migration process is in fact induced by the deposition of the top metal layer. However, it is still justified since, as will be shown later in this report, the driving force for the migration of PEG results from the new equilibria operating on the system upon metal evaporation. Thus, in the present paper, we identify the parameters which control the spontaneous migration of PEG to the blend/metal interface during metal evaporation and determine their effect on the work function of the deposited electrode. We focus on P3HT:PEG films containing no PCBM electron acceptor so that the morphology, optical properties and device performances are modulated *only* by the PEG migration. Under such conditions, the open-circuit voltage is determined directly by the effective work function of the electrodes. Using AFM, HRSEM and XPS we investigated the correlation between the extent of PEG migration and its effect on the electrode work function with the initial PEG concentration, the type of underlying substrate and the type of evaporated metal.

## Experimental

### Materials

Poly(3-hexylthiophene) (P3HT) (Sepiolid P100, regioregularity >95%) was purchased from Rieke Metals and used as received. Poly(3,4-ethylenedioxythiophene): polystyrene sulfonic acid (PEDOT:PSS) was acquired from Haraeus (Clevios PVP AL 4083) and was filtered through a 0.45 μm poly(tetrafluoroethylene) (PTFE) filter before use. Poly(ethylene glycol) (PEG) 200 g/mole Mw was purchased from Fluka and used as received.

### Film deposition and device fabrication

ITO-covered glass substrates were cleaned by sonication in acetone, methanol, and 2-propanol, followed by 15 min of a UV-ozone treatment. PEDOT:PSS, when applied, was spin coated at 5000 rpm onto the ITO/glass and dried at 120 °C for 15 min in ambient conditions. To a toluene solution of P3HT (40 mg/ml) calculated amounts of PEG were added to obtain solutions with 0, 9, 15, 20 or 30 wt% PEG. P3HT:PEG blend films were deposited by spin coating at 2000 rpm for 100 sec onto ITO or ITO/PEDOT:PSS substrates. Thermal deposition of the top metal layer, Al, Au or Ca, was conducted through a shadow mask at a system pressure of ~$10^{-6}$ Torr. For the XPS measurements the thickness of the metal layer was ~3nm. For the devices the thickness of Al cathodes was 90 nm topped by ~10 nm of Au directing a device area of 3 $mm^2$. The samples used for HRSEM cross section imaging were covered by ~100 nm thick conductive layer of Au and cleaved in ambient conditions.

### Characterization

Surface morphology analysis was performed by atomic force microscopy (AFM) in Tapping mode using a Dimension 3100 Nanoscope IIIa (Veeco Instruments). All images were captured at a scan rate of 1–2 Hz and a pixel resolution of 512 × 512.

The absorption spectra were measured using a Varian Cary 100 Scan UV-vis spectrophotometer in the 400-700 nm range.

High-resolution cross section images of cleaved samples were obtained using the Zeiss Ultra Plus high resolution Scanning electron microscope (HRSEM), equipped with a Schottky field emission electron source. The images were acquired using both secondary electrons (in-lens detector) and backscattered electrons (in-lens detector), at a relatively low accelerating voltage of 1.5–2 kV and at working distances of ~2 mm.

X-ray Photoelectron Spectroscopy (XPS), was performed in a Thermo VG Scientific Sigma Probe fitted with a monochromatic Al Kα (1486.6 eV) source. A 100W X-ray beam of 400 μm in diameter was used for high energy resolution scans of the C1s spectra with a pass energy of 30eV. Line-shape analysis was done using the XPSPEAK4.1 software after a Shirley-type background subtraction. The binding energy scale calibration of the C1s spectra was done by referencing the C-C/C-H bond signal to 285eV. For all samples, the C1s spectra were measured in the standard- and bulk-sensitive modes, i.e. with the angle between the direction of the analyser and the specimen normal in the range 53°±30° or 30.5° ±7.5°, respectively. We used the bulk sensitive mode to obtain maximum depth information and to enhance the contribution from the blend/electrode interface region relative to the contribution of the electrode's carbon-based surface contamination. The higher intensity of the C-O peak (286.6 eV) obtained in the bulk-sensitive measurement, compared to that obtained in the standard mode measurement (Figure S1 in the Supporting information section), clearly indicates that the main origin of the C-O signal is from the buried organic/metal



 

interface and not from contaminations at the metal surface. Generally, the C1s spectra of the metal covered blend films were line-fitted to three main peaks: 285 eV (C-C/C-H), 286.6 eV (C-O) and 288.6 eV (O-C=O). However, in the case of the highly reactive Ca, known to attract carbonate ($CO_3^{-2}$) contamination, the C1s XPS spectra were line fitted with an additional 289.5 eV carbonate peak. Line fitting examples for Al-covered and Ca-covered samples are shown in Figure S2 and S3 of the Supporting information section, respectively. Based on inelastic mean free path estimations of the metal/blend system, the information depth of C1s electrons includes a ~5nm thick organic film beneath the Al layer.[26] For quantitative XPS analysis of the surface composition, we compared only samples with identical metal coverage, i.e. samples that were together in the evaporation chamber. For such a set of samples we normalised the intensity of the C1s spectra to the area under the peak of the relevant metal (Al 2p, Ca 2p or Au 4f). The area under the metal peak represents the thickness of the metal overlayer and is constant for each set of samples.

Device characterization was performed in inert atmosphere under 100 mW/cm$^2$ AM1.5G class A sun simulator (Science Tech Inc. ss150 solar simulator) with a Keithley 2400 source meter.

## Results and discussion

To study the metal evaporation-induced additive migration we spun films from solutions containing known quantities of low-Mw (200 g/mole) PEG and P3HT onto either ITO/PEDOT:PSS or ITO substrates. PEG was used as the additive for two main reasons: i) the presence of a PEG interlayer at the organic/electrode interface was shown by us and others to increase both Voc and Jsc [15, 27]; and ii) the surface energy of PEG, ~43 mJ m$^{-2}$,[28] is higher than that of both P3HT (~27 mJ m$^{-2}$ )[29] and PCBM (~38 mJ m$^{-2}$)[29] and therefore it is not expected to enrich the blend/air interface during spin-coating. This combination of features makes it a most suitable candidate to study the migration of additives to the polymer/metal interface induced by the metal evaporation. In this study P3HT:PEG blends were used with no PCBM so that the system is kept simple and PEG migration could be carefully followed and understood. The P3HT:PEG blend films were subjected to a series of measurements, prior to and after metal evaporation, to examine the composition of the blend surface before and after metal deposition.

The surface topography of P3HT:PEG films spun on ITO/PEDOT:PSS or ITO substrates as a function of PEG content is first studied by AFM. As shown in Figure 1Figure , the P3HT:PEG films exhibit macroscopic wave-like surface topography with circular depressions. These features are independent of substrate type, and their size increases with increasing PEG content. Such a surface topography is typical of the complex interplay between wetting and phase separation of immiscible polymer blends. [30, 31] Under such conditions the polymer blend undergoes lamellar (vertical) phase separation, with the lower polymer layer dewetting from the bottom substrate forming a wave topography. The upper polymer layer conformally follows the bottom layer topography. [29, 31-34] The observation of identical wave-like surface topography on both substrates reveals that a similar vertical phase separation occurs in the P3HT:PEG blends spun on both substrates during film formation. An illustration of the P3HT:PEG bilayer is provided in the Supplementary Information section (Figure S4).

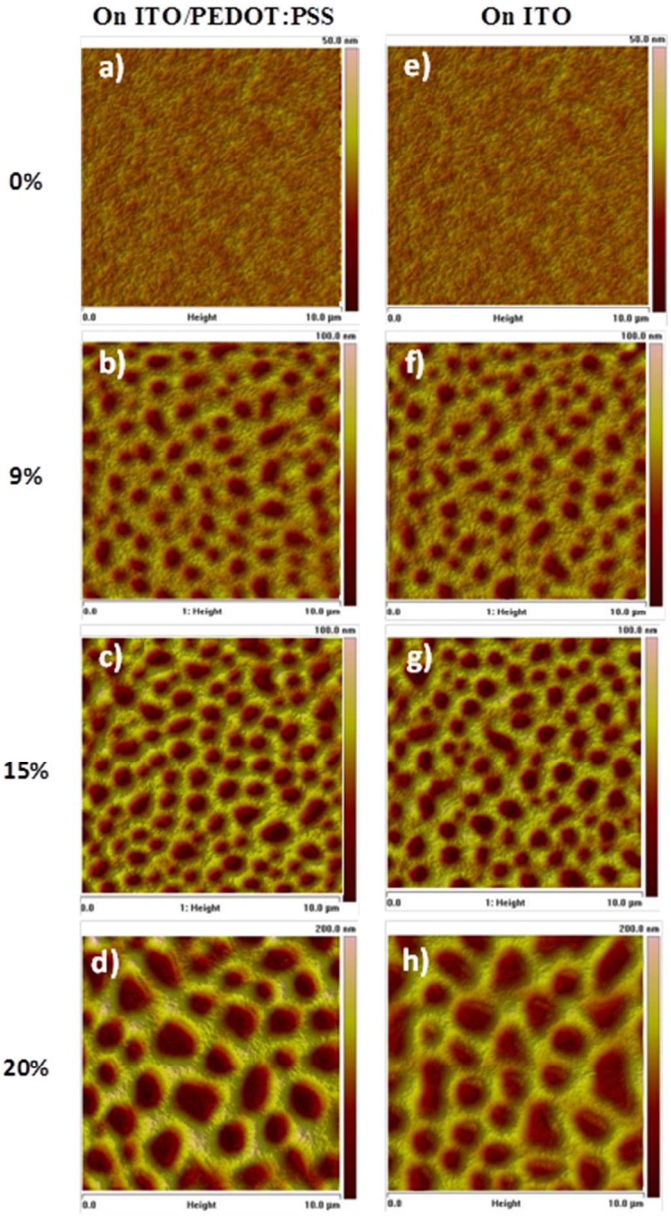


Figure 1- AFM surface topography images of P3HT:PEG films with 0, 9, 15 or 20 wt% PEG on ITO/PEDOT:PSS (a-d) and ITO (e-h): (AFM line profiles are shown in Figure S5 of the Supporting Information)

To further investigate the P3HT:PEG separation during film formation optical absorption measurements were performed on films spun from the P3HT:PEG blends on ITO and ITO/PEDOT:PSS, and the normalized spectra are presented

in Figure 2. The non-normalized absorption spectra are compared in the Supplementary Information section, Figure S6, and indicate a slight reduction (< 10%) in film thickens with the increase of PEG content. Films spun from the same solutions on both substrates generated highly similar absorption spectra. All absorption spectra of the P3HT:PEG films show the well-known features of regioregular P3HT absorption: two main vibronic transitions at 520 and 560 nm, and a shoulder at 605 nm.[32] However, the relative intensities of the vibronic transitions and the shoulder depend on PEG content. More specifically, while the absorption spectra of the films with either no or low concentration of PEG (9 wt%) are highly similar, blends with higher PEG contents (15 and 20 wt%) show a gradual enhancement of the second vibronic peak (560 nm) and the shoulder (620 nm). Further increasing PEG content to 33 wt% did not further amplify the second peak or the shoulder. The increase of the second vibronic peak and the shoulder can be attributed to an increase in P3HT conjugation length and crystallinity induced by phase separation.[33] This phase separation processes, generated by the low miscibility of PEG in P3HT, results in the formation of PEG-rich domains and highly ordered P3HT-rich domains. Importantly, the effect of phase separation-induced crystallization in PEG:P3HT blends is independent of the underlying substrate, ITO/PEDOT:PSS or ITO, as evident by comparing Figure 2a and 2b.

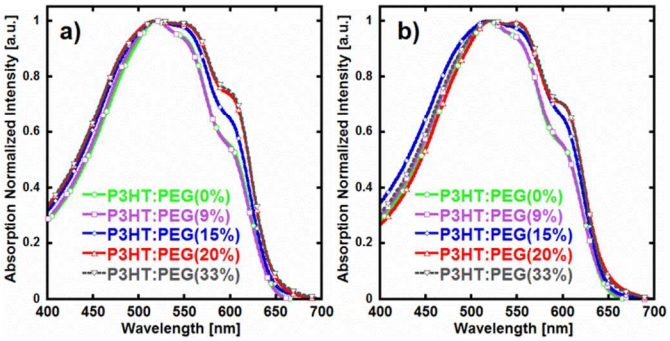


Figure 2 - Normalised Absorption spectra of P3HT: PEG blend films on PEDOT:PSS (a) or ITO (b), with varying PEG content (wt %).

The vertical distribution of the P3HT-rich and PEG-rich domains in the P3HT:PEG spun films is studied using cross section high-resolution scanning electron microscopy (HRSEM). Cross section HRSEM images of a P3HT:PEG film with a high PEG content (20wt%) on ITO/PEDOT:PSS (Figure 3a and 3b) or ITO (Figure 3c and 3d), covered by Au, reveal two distinct polymer layers in the organic film. The same bilayer structure was found for the same film (with high PEG content) also after Al evaporation (Support information Figure S7a). The backscattered images, Figure 3a and 3c (and Figure S7 b), show that the bottom polymer layer has a darker contrast compared to the upper polymer layer. The darker contrast reflects low electron density and hence is assigned to the poorly conducting PEG-rich phase. The bright contrast of the upper polymer layer reflects its high electron density, typical for semiconducting P3HT. This segregation of the blend into two distinct layers is further supported by the secondary electron images, Figure 3b and 3d, where the contrast represents mainly topography. The secondary electron images show that the top metal coating and upper polymer layer cross-sections are characteristic of abrupt brittle fractures, while the edge of the bottom polymer layer is characteristic of plastically deformed ductile fracture. These observations are in good agreement with the glass transition temperatures (Tg) of PEG (-85°C) [34] and P3HT (~110°C) [35] suggesting that the mechanical cross sectioning at room temperature caused a brittle fracture of the P3HT-rich (upper) layer and a ductile fracture of the PEG-rich (lower) layer.

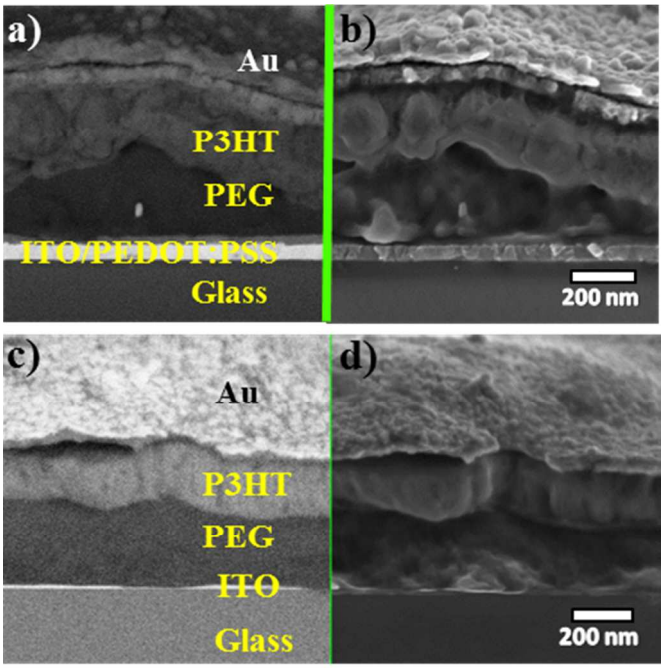


Figure 3- HRSEM cross section backscattered electrons (a and c) and secondary electrons (b and d) images of P3HT:PEG (20 wt %) films spun on ITO/PEDOT:PSS (a and b) or ITO (c and d). The organic layer is covered with a ~100 nm of Au for conductivity.

The phase separation of the P3HT:PEG blend during spin coating into distinct domains aligned parallel to the surface reflects the lack of solubility and the differences in the surface energies of PEG and P3HT.[30] The component with the lower surface energy, P3HT (~27 mN/m$^2$) [28], generally segregates to the film surface to minimize the air/polymer interfacial energy, and PEG, with the higher surface energy (~43 mN/m$^2$) [27], is present on the substrate. It is also evident from Figure 3 that the wave-like morphology of the bottom PEG-rich layer is translated through the P3HT-rich layer to the film surface, as observed in the AFM images (Figure 1). The combination of AFM and HRSEM measurements indicate that the surface roughness and the thickness of the bottom PEG-rich layer increase with PEG content in the blends. These experimental

results support the theoretical expectation of P3HT:PEG phase separation during spin coating into an ordered P3HT-rich layer at the organic/air interface, and a wavy PEG-rich layer at the organic/substrate interface. We note that this distinct layered structure is obtained on both ITO/PEDOT:PSS and ITO substrates.

While these results, which are supported by sound free energy considerations, clearly indicate that PEG does not enrich the film surface, several studies have reported the presence of PEG at the top organic/metal interface in P3HT:PCBM OPV devcies.[19,20,23] In a previous report we showed, based on surface analysis, that although PEG does not enrich the organic surface *during spin coating*, a PEG interlayer is indeed formed by migration to the organic/metal interface but *as a result of the evaporation of the metal contact*.[25]

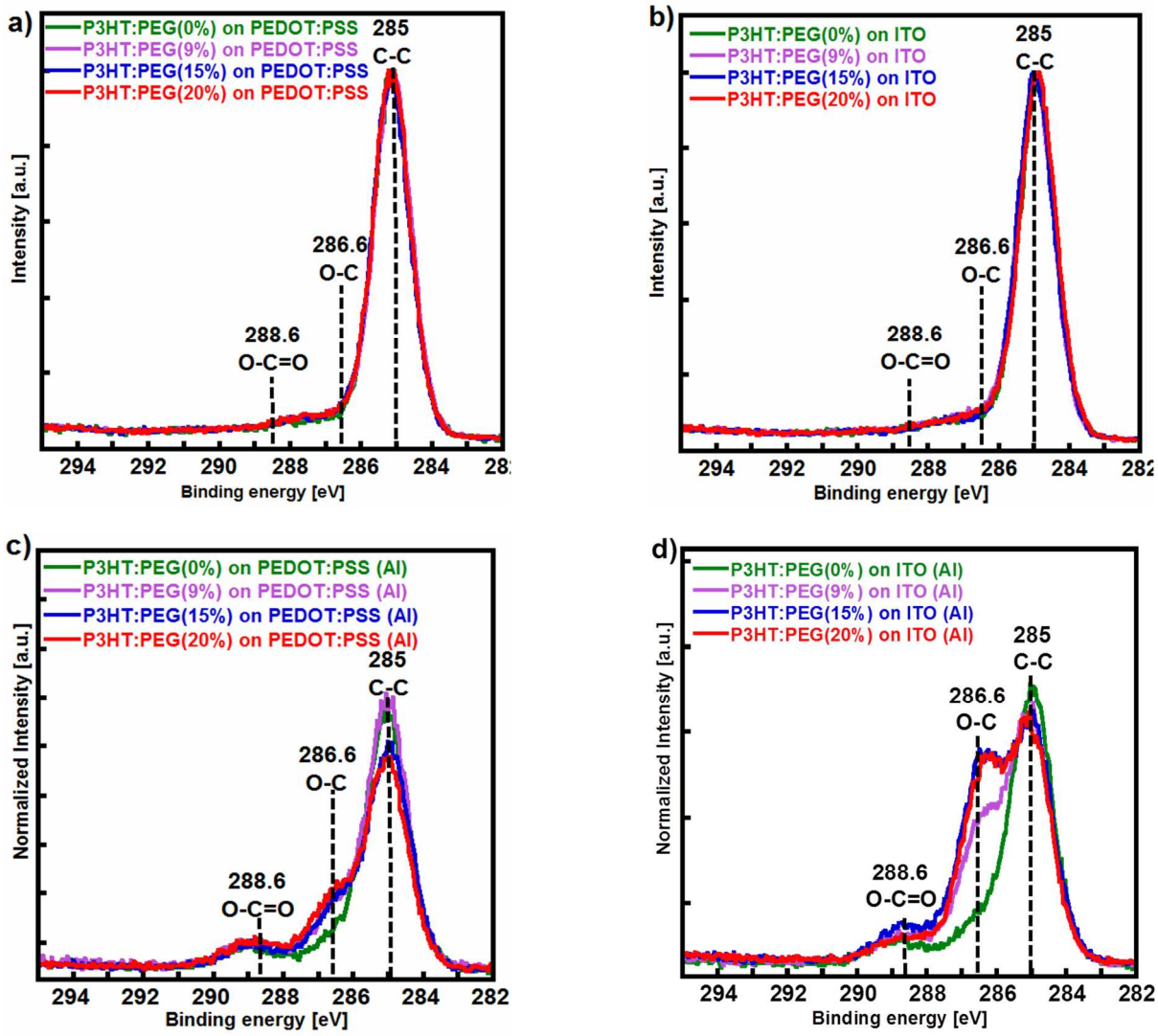


Figure 4- Normalised high energy resolution C1s XPS spectra measured in standard mode of the bare (a and b) and Al-covered (c and d) surface of P3HT:PEG blends deposited on ITO/PEDOT:PSS (a and c) or ITO (b and d).

We further investigate the metal evaporation-induced PEG migration by comparing the X-ray Photoelectron Spectroscopy (XPS) spectra of P3HT:PEG blend surfaces before and after metal deposition. Thin strips of Al were thermally evaporated onto the P3HT:PEG blend films deposited on ITO or ITO/PEDOT:PSS substrates. The evaporation time was extremely short, less than 30 sec, and the samples' temperature was kept below 25°C. No further annealing process was performed. Notably, the Al layer was thin enough, ~3 nm, to allow XPS characterization of the underlying blend/Al interface by performing the measurement through the Al layer. Presence of PEG at the organic/metal interface is associated with the C-O peak at 286.6 eV in the XPS spectrum which is characteristic of the pristine PEG in C1s XPS spectrum.[36] The peak at 286.6eV binding energy could also be attributed to the interaction of Al atoms with bulk adsorbed oxygen and the polymer to form an Al–O–C complex,[37-39] or due to organic contaminants adsorbed on the sample's surface. The contribution of these

species is represented in the intensity of the C-O peak in the XPS spectra of pristine P3HT films with no PEG. Namely, comparing the intensity of the 286.6eV XPS peak of the bare pristine P3HT film and that covered with Al (see blue lines in Figure S2a and S2b in the Supporting information) clearly shows that the contribution of these species to the C-O peak is minor. Furthermore, the small peak at 288.6 eV (magenta line in Figure S2 in the Supporting information), associated with O–C=O bonds resulting from unintentional oxidation or contamination of the surfaces, did not show significant changes in all XPS spectra revealing similar low contamination levels in all films. Accordingly, we can state unambiguously that any increase of the C-O peak intensity over the values attained for the pristine-P3HT films provides direct evidence for the increase in PEG concentration at the blend/Al interface."

Figure 4 shows the XPS spectra measured in the standard mode (see experimental section) on the bare organic surfaces, Figure 4a and 4b, and of an adjacent area that is buried under the Al stripe, Figure 4c and 4d. Clearly, all XPS spectra of the bare organic surfaces are identical for all films regardless of PEG content and type of underlying substrate, and show no evidence of PEG at the surface. In contrast, the XPS spectra of the organic surfaces under the Al-contacts are strongly dependent on PEG content in the film. More specifically, Figure 4c and 4d show a noticeable increase of the C-O peak at 286.6 eV, associated with the PEG, with an increase of PEG content. The comparison of standard and bulk-sensitive mode XPS measurements (see the Supporting information Figure S1) confirms that the main C–O intensity increase is due to the PEG species present at the organic/Al interface and not to contaminations at the Al/air interface. Also, the comparison between the XPS spectra of the same film either bare or covered by a thin Al layer reveals the presence of PEG at the organic/Al interface but not at the organic/air interface. Previous reports have shown that thermally deposited Al, characterised by a low reduction potential (-1.66 V)[40], tends to react with PEG.[41] Therefore, we speculate that PEG migration to the organic/Al interface is induced by the interfacial reaction between the hydroxyl-terminated groups of PEG and the thermally evaporated Al atoms. The formation of the metal-organic complex[42] reduces the interfacial energy and hence acts as the driving force for PEG migration to the organic/Al interface. Although the reduction in film thickness could assist PEG migration, the dramatic differences in the XPS spectra of the blends (well over 10%) could not be solely assigned to the reduction in film thickness. Importantly, while the morphology, stratification and surface composition of the spun P3HT:PEG films are independent of the underlying substrate, this is not the case after metal evaporation, as evident by comparing Figures 4c and 4d. Notably, the C-O peak intensity in the XPS spectra increases sharply for blend films on ITO substrates but only increases gradually for blend films on ITO/PEDOT:PSS substrates. In other words, the PEG content at the organic/Al interface of a blend film spun on ITO/PEDOT:PSS is substantially lower than that obtained for the same blend spun on ITO. Moreover, even high-PEG content P3HT:PEG(20%) blends on ITO/PEDOT:PSS had significantly less PEG at the organic/Al interface than low-PEG content P3HT:PEG(9%) blends on an ITO substrate. These results indicate that the migration of PEG to the organic/Al interface during Al evaporation is modulated by the degree of PEG/substrate affinity. The surface energy of the substrate, and in particular its polar component, determines the strength of interaction between the substrate and the polar hydroxyl-terminated PEG groups.[43] Hence, comparing PEDOT:PSS, with a surface energy of ~67 mJ/m$^2$ and polar component of ~37 mJ/m$^2$, to ITO, with a surface energy of ~55 mJ/m$^2$ and polar component of ~20 mJ/m$^2$, emphasises the stronger attraction of PEG to PEDOT:PSS than ITO.[44] The strong interaction between PEG and PEDOT:PSS results in a competition between the association of PEG to the PEDOT:PSS/organic bottom interface and its attraction to the organic/Al interface during Al evaporation. This competition is reflected in the gradual accumulation of PEG at the organic/Al interface with increased PEG content in the blend. In contrast, ITO-PEG interactions are substantially weaker than those of PEG-Al and hence Al deposition induces strong migration of PEG to the organic/Al interface reflected in a sharp increase of PEG content at the organic/Al interface.

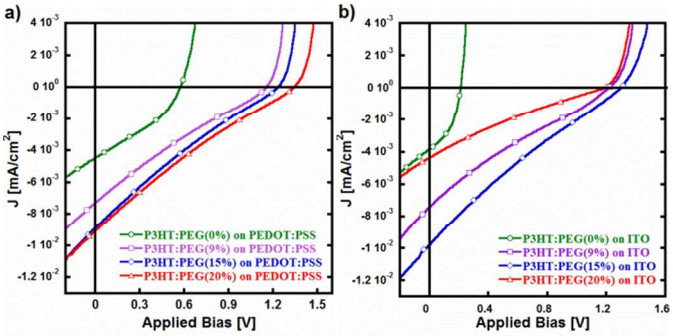


Figure 5: Current density-voltage (J-V) curves measured under illumination of P3HT:PEG films with different PEG content. The general device structure is: (a) ITO/PEDOT:PSS/P3HT:PEG/Al; and (b) ITO/P3HT:PEG/Al. (J-V curves measured in the dark are shown in Figure S8 of the Supporting Information)

The competition between the attraction of PEG to the underlying substrate and its migration to the organic/metal interface during metal deposition is also reflected in the current density-voltage (J-V) measurements of photodiodes composed of the P3HT:PEG films. The absence of an electron acceptor considerably limits the photocurrent generation resulting in extremely low current densities. Nevertheless, the simplicity of the system with only one electronically contributing component in the active layer, P3HT, allows us to correlate the organic/Al interface composition with the Voc. Whereas in standard BHJ devices the Voc depends not only on the electrode work functions but also on the energy levels of the donor and acceptor species, in our model P3HT-only devices the Voc is

strictly correlated with the electrode work function, and hence is a direct probe of the organic/electrode interface.[45, 46] The results presented in Figure 5 show that in all the device configurations we measured, the addition of PEG to P3HT always resulted in a significant enhancement of Voc. The increase of Voc with increasing PEG content is in good agreement with previous studies in which a PEG interlayer was added on top of the P3HT:PCBM blend.[15] In these studies, the higher Voc was attributed to the decrease of the Al work function due to interactions with the ethylene oxide groups of PEG.[15, 27, 47, 48] Notably, the increase in Voc observed in this study, up to 1V, is substantially higher than the 0.15V observed for P3HT:PCBM:PEG devices and is solely a consequence of the decrease of the Al work function.

In good agreement with the XPS results, the increase in Voc with PEG content is gradual in devices on ITO/PEDOT:PSS, but step-like in devices on ITO. Namely, in devices using a ITO/PEDOT:PSS bottom electrode the Voc increases gradually with PEG content from 0.6 V for P3HT (0% PEG) to 1.3 V for P3HT:PEG(20wt%) (Figure 5a). While in devices using an ITO bottom electrode the Voc is 0.2 V for P3HT, but ~1.2 V for all PEG containing blends. Since we showed above (Figures 1, 2 and 3) that the morphology and absorption spectra are independent of the underlying substrate, we can confidently state that the migration of PEG to form an interlayer during metal deposition is a result of the competition between metal-PEG and substrate-PEG interactions.

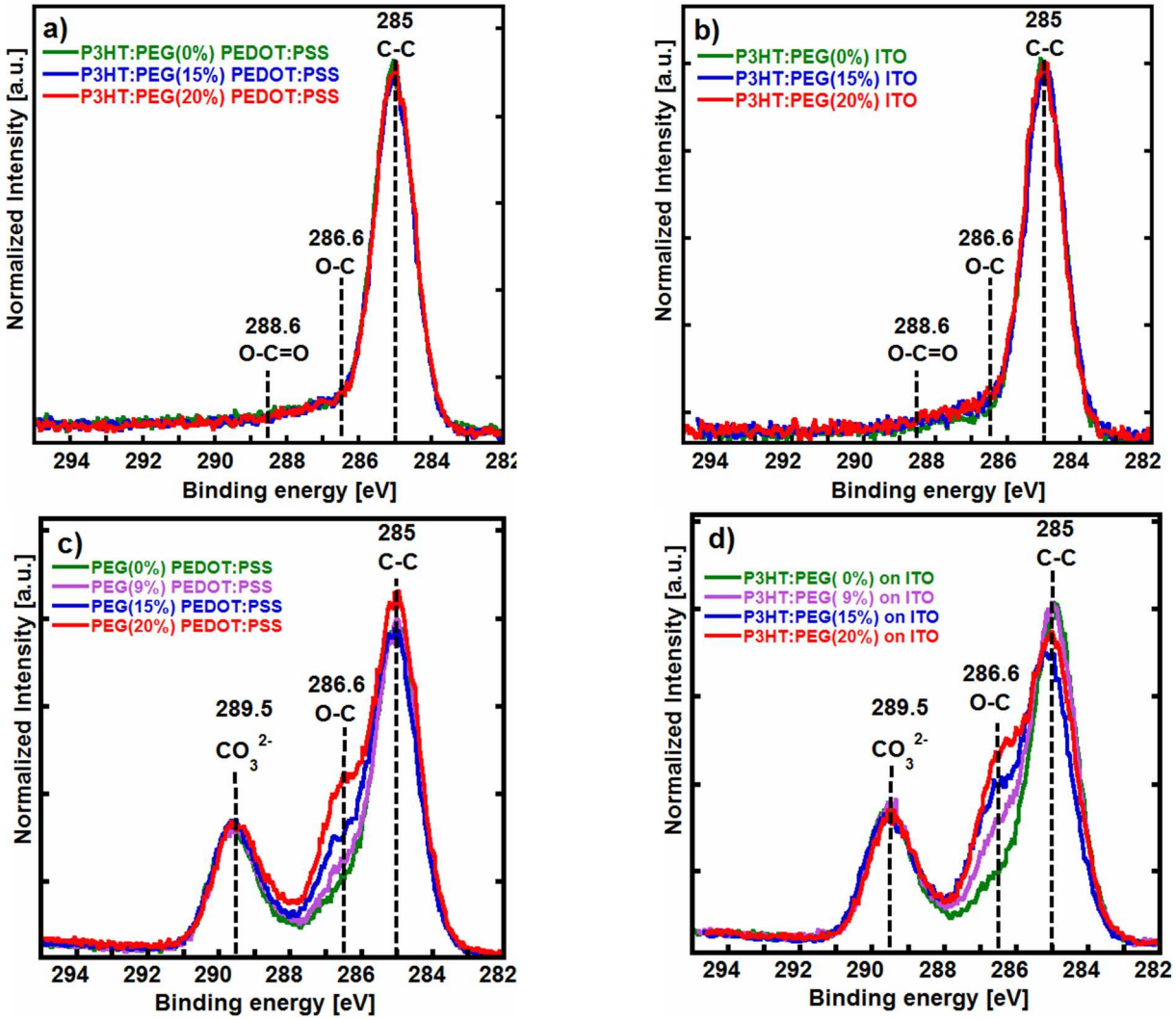


Figure 6- Normalised high energy resolution C 1s XPS spectra measured in standard mode of Au-covered (a and b) or Ca-covered (c and d) P3HT:PEG films deposited on ITO/PEDOT:PSS (a and c) or ITO (b and d).

To confirm that PEG migration to the blend/metal interface during electrode evaporation competes with PEG-substrate interactions, we replaced Al, a reactive metal, with an inert metal, Au (reduction potential 1.5 V),[40] or a highly reactive metal, Ca (reduction potential -2.87 V),[40]. The Au and Ca layers were again thin enough (~3nm) to enable XPS characterization of the organic/metal interface. Again, the C1s XPS spectra on the bare organic surfaces and those under the Au or Ca stripes were compared. The XPS spectra of bare organic surfaces were identical to the bare surfaces measured in

the Al experiment (Figures 4a and 4b), showing no evidence of PEG at the organic/air interface (Figure S9, Supporting information). The XPS spectra of Ca covered areas (Figure 6c and 6d) however, show a substantial increase in PEG content at the organic/Ca interface. The similar C-O peak intensities obtained from films deposited on both ITO and ITO/PEDOT:PSS substrates indicates that the PEG/Ca interactions dominate over PEG/substrate interaction. This can be explained by the extremely low reduction potential of Ca (-2.87 V) which leads to a strong attraction of PEG to the deposited Ca. The PEG-Ca interaction substantially reduces the interfacial energy and acts as the dominant driving force for migration and accumulation of PEG at the organic/Ca interface. In contrast to Ca, the intensity of the PEG C-O peak is negligible for all Au covered samples regardless of the initial PEG concentration and the type of the substrate clearly indicating that PEG is not present at the organic/Au interface. Unlike Ca, Au has a high reduction potential (1.5 V) that renders it inert to PEG with no driving force for PEG migration to the organic/Au interface.

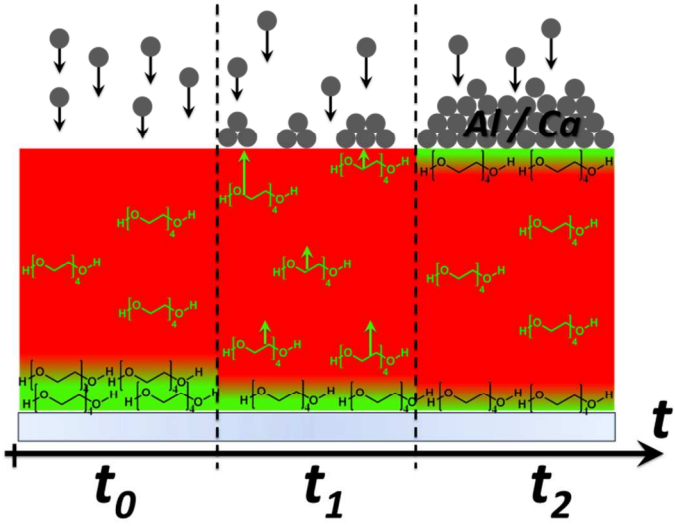


Figure 7- An illustration of the suggested spontaneous interlayer formation by PEG migration due to PEG-metal interactions.

Importantly, the comparison between Ca, Al and Au allows us to rule out the possibility that PEG migration to the organic/metal interface is a result of local heating during the thermal deposition of the metal. If local thermal heating were the driving force, the migration of PEG to the interface would be independent of metal reduction potential and would have occurred for all deposited metals. However, since Au-covered samples show no PEG at the blend/Au interface, we can rule out thermal heating as the driving force.

Finally, a suggested mechanism for PEG migration toward the organic/metal interface during the metal (Ca or Al) deposition is illustrated in Figure 7. We speculate that during spin coating of the P3HT:PEG blends, the high surface energy of PEG directs its segregation to the bottom blend/substrate interface forming the bilayer P3HT(top):PEG(bottom) morphology seen in the HRSEM images in Figures 3 and S7. Some PEG molecules, up to its solubility limit in P3HT, are retained and homogenously dispersed in the film. The concentration of the dispersed PEG molecules is extremely low, below the XPS detection limit (>0.1at %) and hence not detectable in the XPS of the bare organic surfaces (Figure 4a and 4b). This initial structure of the film prior to metal deposition is illustrated in the left panel of Figure 7 ($t_0$). During the metal evaporation, the first Al atoms reaching the organic surface interact with PEG molecules that are close to the surface to significantly reduce the interfacial energy. Further evaporation and metal-PEG interactions generate a gradient of PEG concentration close to the surface which induces the diffusion of PEG molecules from the film to the new metal/organic interface ($t_1$ in the scheme). This migration could also include molecules from the bottom PEG layer, but the concentration gradient pulling PEG to the upper interface is modulated by PEG affinity to the bottom substrate. Finally, once a PEG monolayer at the blend/metal interface is completed, the driving force for migration is terminated. While some PEG is still suspended in the film, the Al-PEG interlayer at the upper interface is sufficient to dramatically decrease the Al work function.

## Conclusions

In summary, we used P3HT:PEG films to investigate the fundamentals of the metal evaporation-induced additive migration to the organic/metal interface. This process, which leads to the spontaneous formation of a PEG interlayer, reduces the metal's work function and results in a significant increase of Voc is strongly affected by the complex interplay between the affinity of the additive to the underlying substrate and to the evaporated metal. Although the morphology of the P3HT:PEG films deposited from toluene is different from that of P3HT:PCBM:PEG films deposited from DCB, they are still a good model system to provide insight on additive migration in "real" OPVs and in other organic electronic devices. We therefore suggest that judicious selection of additives based on their affinity to the evaporated electrodes and the substrate could be used to direct spontaneous formation of interlayers to tune the electrode work function in OPVs and other organic electronic devices. Importantly, this study also demonstrates that surface composition and bulk morphology are significantly affected by the metal deposition process. This should be seriously considered when correlating structure and performance.

## Acknowledgements

We thank Dr. L. Kornblum for fruitful discussions and helpful suggestions. This research was partially supported by the Israeli Nanotechnology Focal Technology Area project on "Nanophotonics and Detection" and the Helmsley Alternative

Energy series of the Technion, Israel Institute of Technology, and the Weizmann Institute of Science.

## Notes and references

[a] *Department of Materials Science and Engineering, Technion – Israel Institute of Technology, Haifa 32000, Israel Fax: +972-4-8295677; Tel: +972-4-8294572; E-mail: gitti@tx.technion.ac.il*
[b] *The Solid State Institute, Technion – Israel Institute of Technology, Haifa 32000, Israel*

Electronic Supplementary Information (ESI) available: XPS spectra in the standard and bulk mode of P3HT:PEG blends; line fitting and normalised XPS spectra in standard mode; AFM line profiles, dark current density – voltage curves; non-normalized UV-Vis absorption spectra; HRSEM images of the Al-covered films.

1. M. A. Green, K. Emery, Y. Hishikawa, W. Warta and E. D. Dunlop, *Progress in Photovoltaics: Research and Applications*, 2014, **22**, 1-9.
2. H.-Y. Chen, H. Yang, G. Yang, S. Sista, R. Zadoyan, G. Li and Y. Yang, *The Journal of Physical Chemistry C*, 2009, **113**, 7946-7953.
3. A. Tada, Y. Geng, M. Nakamura, Q. Wei, K. Hashimoto and K. Tajima, *Physical chemistry chemical physics : PCCP*, 2012, **14**, 3713-3724.
4. A. Pivrikas, H. Neugebauer and N. S. Sariciftci, *Solar Energy*, 2011, **85**, 1226-1237.
5. S. J. Lou, J. M. Szarko, T. Xu, L. Yu, T. J. Marks and L. X. Chen, *J Am Chem Soc*, 2011, **133**, 20661-20663.
6. K. R. Graham, P. M. Wieruszewski, R. Stalder, M. J. Hartel, J. Mei, F. So and J. R. Reynolds, *Advanced Functional Materials*, 2012, **22**, 4801-4813.
7. Q. Tai, J. Li, Z. Liu, Z. Sun, X. Zhao and F. Yan, *Journal of Materials Chemistry*, 2011, **21**, 6848-6853.
8. D. H. Wang, Y. Kim do, K. W. Choi, J. H. Seo, S. H. Im, J. H. Park, O. O. Park and A. J. Heeger, *Angew Chem Int Ed Engl*, 2011, **50**, 5519-5523.
9. S. S. Sharma, G. D. Sharma and J. A. Mikroyannidis, *Solar Energy Materials and Solar Cells*, 2011, **95**, 1219-1223.
10. Z. X. Xu, V. A. Roy, K. H. Low and C. M. Che, *Chem Commun* 2011, **47**, 9654-9656.
11. T. Akira, G. Yanfang, W. Qingshuo, H. Kazuhito and T. Keisuke, *Nature Materials*, 2011, **10**, 450-455.
12. Y. Zhou, C. Fuentes-Hernandez, J. Shim, J. Meyer, A. J. Giordano, H. Li, P. Winget, T. Papadopoulos, H. Cheun, J. Kim, M. Fenoll, A. Dindar, W. Haske, E. Najafabadi, T. M. Khan, H. Sojoudi, S. Barlow, S. Graham, J. L. Bredas, S. R. Marder, A. Kahn and B. Kippelen, *Science*, 2012, **336**, 327-332.
13. P. G. Karagiannidis, N. Kalfagiannis, D. Georgiou, A. Laskarakis, N. A. Hastas, C. Pitsalidis and S. Logothetidis, *Journal of Materials Chemistry*, 2012, **22**, 14624.
14. H.-L. Yip, S. K. Hau, N. S. Baek, H. Ma and A. K. Y. Jen, *Advanced Materials*, 2008, **20**, 2376-2382.
15. F. Zhang, M. Ceder and O. Inganäs, *Advanced Materials*, 2007, **19**, 1835-1838.
16. C. Goh, S. R. Scully and M. D. McGehee, *Journal of Applied Physics*, 2007, **101**, 114503.
17. C. Waldauf, M. Morana, P. Denk, P. Schilinsky, K. Coakley, S. A. Choulis and C. J. Brabec, *Applied Physics Letters*, 2006, **89**, 233517.
18. K. Asadi, P. de Bruyn, P. W. M. Blom and D. M. de Leeuw, *Applied Physics Letters*, 2011, **98**, 183301.
19. J. W. Jung, J. W. Jo and W. H. Jo, *Adv Mater*, 2011, **23**, 1782-1787.
20. A. Tada, Y. F. Geng, M. Nakamura, Q. S. Wei, K. Hashimoto and K. Tajima, *Physical Chemistry Chemical Physics*, 2012, **14**, 3713-3724.
21. F. C. Chen and S. C. Chien, *Journal of Materials Chemistry*, 2009, **19**, 6865-6869.
22. H. Kang, J. Lee, S. Jung, K. Yu, S. Kwon, S. Hong, S. Kee, S. Lee, D. Kim and K. Lee, *Nanoscale*, 2013, **5**, 11587-11591.
23. K. Tajima and K. Hashimoto, *Chemical record*, 2011, **11**, 8-17.
24. Q. Wei, T. Nishizawa, K. Tajima and K. Hashimoto, *Advanced Materials*, 2008, **20**, 2211-2216.
25. I. Dekman, R. Brener and G. L. Frey, *Journal of Materials Chemistry C*, 2013.
26. S. Tanuma, C. J. Powell and D. R. Penn, *Surface and Interface Analysis*, 1991, **17**, 927-939.
27. S.-C. Chien, F.-C. Chen, M.-K. Chung and C.-S. Hsu, *The Journal of Physical Chemistry C*, 2012, **116**, 1354-1360.
28. C. J. van Oss, M. K. Chaudhury and R. J. Good, *Advances in Colloid and Interface Science*, 1987, **28**, 35-64.
29. D. M. DeLongchamp, R. J. Kline and A. Herzing, *Energy & Environmental Science*, 2012, **5**, 5980.
30. G. Krausch, *Materials Science and Engineering: R: Reports*, 1995, **14**, 94.
31. K. Tanaka, A. Takahara and T. Kajiyama, *Macromolecules*, 1996, **29**, 3232-3239.
32. T.-A. Chen, X. Wu and R. D. Rieke, *Journal of the American Chemical Society*, 1995, **117**, 233-244.
33. K. Zhao, Z. Ding, L. Xue and Y. Han, *Macromol Rapid Commun*, 2010, **31**, 532-538.
34. S. Unal, Q. Lin, T. H. Mourey and T. E. Long, *Macromolecules*, 2005, **38**, 3246-3254.
35. Y. Kim, S. A. Choulis, J. Nelson, D. D. C. Bradley, S. Cook and J. R. Durrant, *Applied Physics Letters*, 2005, **86**, 063502.
36. G. Beamson and D. Briggs, *High Resolution XPS of Organic Polymers: The Scienta ESCA300 Database*, John Wiley & Sons, 1992.
37. Q. D. Ling, S. Li, E. T. Kang, K. G. Neoh, B. Liu and W. Huang, *Applied Surface Science*, 2002, **199**, 74-82.
38. D. Chen, A. Nakahara, D. Wei, D. Nordlund and T. P. Russell, *Nano Lett*, 2011, **11**, 561-567.
39. C.-Y. Nam, D. Su and C. T. Black, *Advanced Functional Materials*, 2009, **19**, 3552-3559.
40. D. R. Lide, in *CRC Handbook of Chemistry and Physics version 2008 ed. 84*, ed. L. D.R, CRC Press, 2004, pp. 12-124.
41. M.-W. Lin, T.-C. Wen, Y.-J. Hsu and T.-F. Guo, *Journal of Materials Chemistry*, 2011, **21**, 18840-18846.
42. G. L. Fisher, A. V. Walker, A. E. Hooper, T. B. Tighe, K. B. Bahnck, H. T. Skriba, M. D. Reinard, B. C. Haynie, R. L. Opila, N. Winograd and D. L. Allara, *Journal of the American Chemical Society*, 2002, **124**, 5528-5541.

43. Z. Xu, L.-M. Chen, G. Yang, C.-H. Huang, J. Hou, Y. Wu, G. Li, C.-S. Hsu and Y. Yang, *Advanced Functional Materials*, 2009, **19**, 1227-1234.
44. G. Ho Jung, K.-G. Lim, T.-W. Lee and J.-L. Lee, *Solar Energy Materials and Solar Cells*, 2011, **95**, 1146-1150.
45. C. J. Brabec, A. Cravino, D. Meissner, N. S. Sariciftci, T. Fromherz, M. T. Rispens, L. Sanchez and J. C. Hummelen, *Advanced Functional Materials*, 2001, **11**, 374-380.
46. S. Braun, W. R. Salaneck and M. Fahlman, *Advanced Materials*, 2009, **21**, 1450-1472.
47. F.-C. Chen and S.-C. Chien, *Journal of Materials Chemistry*, 2009, **19**, 6865-6869.
48. J.-Y. Jeng, M.-W. Lin, Y.-J. Hsu, T.-C. Wen and T.-F. Guo, *Advanced Energy Materials*, 2011, **1**, 1192-1198.